RSC Advances

ROYAL SOCIETY OF CHEMISTRY

www.rsc.org/advances

Activity of Faujasite Supported Gold Monomer towards Water Gas Shift Reaction: Hybrid Density Functional Theory/Molecular Mechanics Approach

Subhi Baishya and Ramesh Ch. Deka

Department of Chemical Sciences, Tezpur University, Napaam-784028, Assam, India

Abstract

The activity of faujasite supported neutral and cationic gold monomer towards water gas shift reaction has been investigated with hybrid density functional method. Our calculations indicate that CO adsorption on Au^n/FAU (n=0, +1 and +3) in presence of pre-adsorbed H_2O presents a favorable configuration for studying the water gas shift reaction. Occurrence of high barriers in dissociation of water and the endothermicity of the overall reaction observed in the cationic systems will diminish their activity towards water-gas shift reaction. The rate limiting step in Au^+/FAU is the formation of a carboxyl intermediate. On the other hand, comparatively lower barriers and exothermicity of the reaction in Au^0/FAU indicates it to be a better catalyst. The stability of all the species including the transition states with respect to the interacting species indicates no thermal activation in faujasite supported neutral Au monomer.

1. Introduction

The water gas shift reaction, WGSR ($CO + H_2O \rightarrow CO_2 + H_2$) plays a pivotal role in the chemical industry for H_2 production and hence, designing an improved WGSR catalyst has gained impetus in the present scenario. Various experimental [1-7] and theoretical [8-12] studies have been committed to find a suitable WGSR catalyst. Nano sized gold particles supported on various oxides [13-15] have been appreciated for their unusual and unanticipated catalytic properties at even below room temperature. It has been observed that gold catalysts supported on Fe_2O_3 [16-19], CeO_2 [20-29], TiO_2 [30-35], ZrO_2, Al_2O_3 etc. as well as mixed oxides have [36-41] exhibit excellent catalytic activity towards WGS reaction. Apart from metal oxides, zeolites form an interesting class of solid supports and have been admired due to the presence of pores and cavities of molecular dimensions. In addition, the ability of zeolites to control the particle size and extraordinary thermal stability makes this material a fascinating class of support. However, very few studies have reported the activity of zeolite supported gold catalysts towards WGS reaction [42,43]. Ichikawa and co-workers [42] identified reaction intermediates involved in the WGS reaction on Au^{n+} ($1 \leq n \leq 3$) incorporated into NaY, Na–mordenite, and Na–ZSM-5 by means of *in situ* FT-IR spectroscopy. On Au^{n+}/NaY, a unidentate formate was obtained as a surface intermediate while Au^{+}/Na–mordenite displayed unidentate formate and organic carbonate species. Formation of different carbonate-like species was observed on Au^{n+}/Na-ZSM-5. Their study proved that dual Au^{+} and Au^{0} are the active sites for the WGSR, especially when it encapsulated inside Na-Y zeolite rather than in Na–mordenite and Na–ZSM-5 catalysts.

The morphology and chemical state of the active Au species in the supported Au catalysts has been largely debated [44-46]. Fu et al [44] provided experimental evidence for the role of

oxidized Au in the WGS reaction using Au-ceria catalyst and proposed that the metallic Au^0 particles are mere spectators as their presence does not change the catalytic performance. DFT calculations on the Au-ceria system by Liu et al [47] provided the first theoretical framework to understand the origin of $Au^{\delta+}$ cations and determine whether the size of the active site is a single Au atom or small Au clusters. Their work demonstrated the Au atom is oxidized by ceria even though no direct Ce-Au bonding is present. CO molecules adsorb sufficiently strongly on the Auδ+ ions for subsequent catalysis. They concluded that the active sites in the catalysts are neither single Au atoms nor sizeable Au particles, but ultra-small Au clusters. The unique catalytic activity has been attributed to the presence of empty nonbonding f-states of CeO_2 near the Fermi level that acts as an electron reservoir similar to metals.

One of the current domains in the field of contemporary catalytic research is the concept of single atom catalysis (SAC) [48] since it offers a better solution by significantly reducing the use of precious metal and maximizing the metal utilization efficiency. Lin et al [49] fabricated Ir_1/FeO_x SAC with an exceptionally high activity for WGS, almost 1 order of magnitude higher than its cluster or nanoparticle counterparts. They found that the single atoms contribute ~70% to the total activity. Yang et al [35] reported the catalytic activity of atomically dispersed Au-$(OH)_x$ species on titania towards the low temperature WGS. The authors reported that higher gold loadings resulted in nanoparticles but this did not add to further activity of the atomically bound gold on titania. The dissociation of H_2O on the Au−O−TiO_x sites was found to be facile.

Keeping in view, the importance of single atom catalysis and the scarcity of theoretical studies on zeolite supported systems, for the first time we investigate the catalytic activity of zeolite supported gold monomer towards water gas shift reaction. Moreover, as it has been observed that oxidation state of supported gold clusters affect their catalytic activity, so it is

necessary to consider both neutral and cationic states of the supported gold monomer. In the present work, we have considered the catalytic activity of Au^0, Au^+ and Au^{3+} supported on faujasite zeolite towards water gas shift reaction and the formation of a stable carboxyl intermediate in the reaction mechanism. Comparison of the reaction barriers involved in the different steps of the reaction mechanism indicates better activity of the supported neutral gold monomer.

2. Computational Details

The hybrid quantum mechanics/molecular mechanics calculations are performed using the SIMOMM (Surface Integrated Molecular Orbital Molecular Mechanics) [50] method implemented in GAMESS program [51]. The entire system is partitioned into a small, chemically active part which is the quantum mechanical part and the larger, outer inactive part comprises the molecular mechanical part. Creation of the inner active part from the entire system generates unpaired electrons (dangling bond) on the subsurface atoms in the inner region which must be terminated so that the chemical behavior of the inner region does not differ from the real surface. Hydrogen atoms are used to saturate these dangling bonds and are known as the linked atoms. Geometry optimizations and transition state searches were accomplished with the quadratic approximation method [52] implemented in GAMESS program. The transition states are characterized with the presence of single negative vibrational frequency. The zeolite model used in our work comprises of 642 atoms and an extra-framework Au atom which is divided in to quantum mechanical and molecular mechanical parts (Figure 1). The quantum mechanical (chemically active) part which consists of a six member ring of faujasite zeolite and the Au atom is treated with B3LYP [53,54] functional, 6-31G (d,p) [55] basis set for Si, Al, O, C, H and LANL2DZ [56] basis set incorporating relativistic effective core potential for Au atom. When a

Si atom of the six-membered ring is substituted by an Al atom; it generates an excess negative charge. The Au atom added is in the +1 oxidation state in order to retain the charge neutrality of the system. Accordingly, isomorphous substitution of three Si atoms by Al atoms according to the Löwenstein rule creates Au^{3+}. The water gas shift reaction is modeled to take place within the active region. The rest of the zeolite framework makes up the molecular mechanical (outer inactive) part which is modeled using the MM3 [57] parameter.

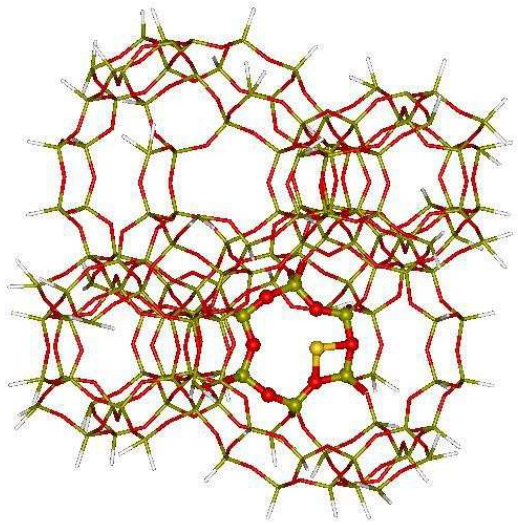

Figure 1: The QM (ball and stick) and MM (stick) regions in the faujasite model used in our work. White-H, Red-O, Green-Si, Yellow-Au.

The binding energy of CO and H_2O has been calculated using equation (1) where, $E_{Au\text{-}A/FAU}$ is the energy of the adsorption complex of A (either CO or H_2O) over faujasite supported Au monomer, $E_{Au/FAU}$ is the energy of faujasite supported Au monomer and E_A is the energy of the free A molecule.

$$BE(A) = (E_{Au/FAU} + E_A) - (E_{Au\text{-}A/FAU}) \quad (1)$$

A positive value of BE corresponds to the formation of stable adsorption complex. In the co-adsorbed aggregates, the binding energy is calculated using:

$$BE(B) = \left(E_{Au\text{-}A/FAU} + E_B\right) - \left(E_{Au\text{-}A,B/FAU}\right) \quad (2)$$

BE(B) is the binding energy of B (CO or H_2O) in the co-adsorbed aggregates, $E_{Au\text{-}A/FAU}$ is the energy of Au/FAU with a pre-adsorbed A molecule, E_B is the energy of free gas phase B molecule and $E_{Au\text{-}A,B/FAU}$ is the energy of the co-adsorbed aggregate. Favorable adsorption of B on Au^n/FAU (n=0, +1 and +3) in the presence of pre-adsorbed A is indicated by positive binding energy value.

3. Results and Discussion

3.1 Faujasite supported gold monomer

The optimized structures of faujasite supported Au monomer in three different oxidation states 0, +1, +3 are shown in Figure 2 and the selected geometrical parameters are summarized in Table 1.

Table 1: Computed selected bond lengths (Å) and NBO charges on faujasite supported Au monomer in three oxidation states.

	Au^0/FAU	Au^+/FAU	Au^{3+}/FAU
	Bond Length		
Au-O_z	2.76	2.30	2.31
Au-Si	3.32	2.98	2.97
Au-Al	-	3.08	2.96
	NBO charges		
q(Au)	-0.026	0.714	0.684

The Au–O_z (O_z represents framework zeolite oxygen), Au-Si and Au-Al distances decrease on moving from neutral to cationic systems. This suggests that the interaction of Au monomer with the faujasite support increases on moving to cationic systems. The frontier molecular orbitals

shown in Figure S1 illustrate the interaction between d-orbital of Au and the p-orbitals of zeolite O-atoms. It can be seen that the overlap of the orbitals is more pronounced in the cationic systems, thereby accounting for their enhanced interaction with the zeolite framework. NBO charge analysis indicates that anchoring of the Au monomer to the faujasite support causes a withdrawal of charge density from the zeolite to the monomer in both neutral and cationic systems evident from the charge carried by the Au monomer. For instance, the NBO charge for neutral Au has been found to be –0.06 e while for the oxidation state of +1, the NBO charge on Au is 0.64 e. It has been observed that the low spin state is more stable than the high spin counterpart.

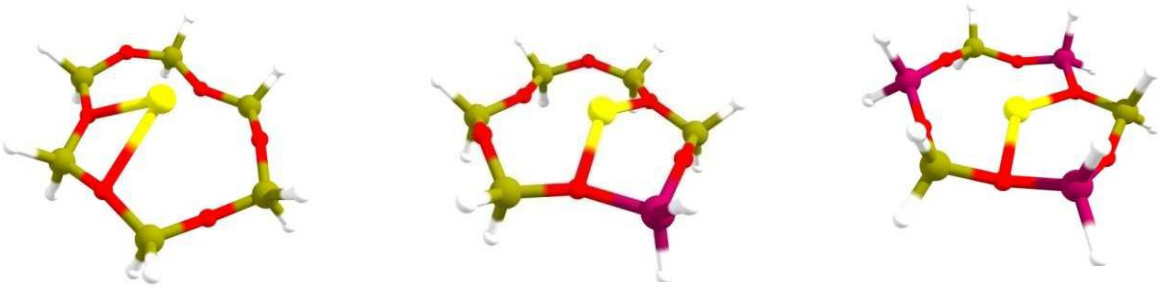

(a) Au^0 /FAU (b) Au^+/FAU (c) Au^{3+}/FAU

Figure 2: Optimized structures of faujasite supported Au monomer. The H, O, Al, Si and Au atoms are depicted by white, red, magenta, green and yellow colors, respectively.

3.2. Adsorption of CO and H_2O on faujasite supported Au monomer:

The optimized structures of CO adsorbed on Au^n/FAU (n=0, +1 and +3) are shown in Figure 3 and the geometrical parameters, vibrational frequency of CO, binding energies and the NBO charges for the CO adsorbed aggregates are summarized in Table 2. Our calculations indicate that the binding energy of CO increases from 3.28 eV in the neutral monomer to 4.59 eV in the +3 oxidation state. Interaction of CO with the Au atom is stronger in the cationic states as revealed from the shorter Au-C bond lengths while the C-O distance does not vary much from

the gas phase value (1.16Å). NBO charges indicate transfer of 0.089e charge to the CO molecule (represented by Δq) as a result of interaction with the gold monomer in Au^0/FAU. The transferred charge goes to the antibonding orbital of CO and consequently the C-O vibrational frequency decreases to 1867.22 cm^{-1} from a value of 2072.23 cm^{-1} observed for the free gas phase CO. On the other hand, in the cationic systems, there is withdrawal of charge from CO reflected from the negative values of Δq. Consequently, the vibrational frequency of CO in the cationic systems increases as compared to the gas phase value. It can be seen from the optimized structures that CO adsorbs in a bent fashion in the neutral monomer while in the cationic systems, it adsorbs as a linear structure. The adsorbed CO interacts with the Au centre via the C atom and it involves overlap of the Au d-orbital and P-orbital of C as depicted in the frontier orbitals shown in Figure S2. The Au-O_z bond length decreases on going to higher oxidation states having a value of 2.04Å in the +3 oxidation state. Our calculated Au–O_z distances of supported cationic gold monomer are in good agreement with the experimental EXAFS value of 2.08 Å in NaY zeolite supported cationic gold atoms [58]. Thus, the interaction of the gold atom with the support increases on moving to higher oxidation states, which is also revealed from the decreasing Au-Al and Au-Si distances.

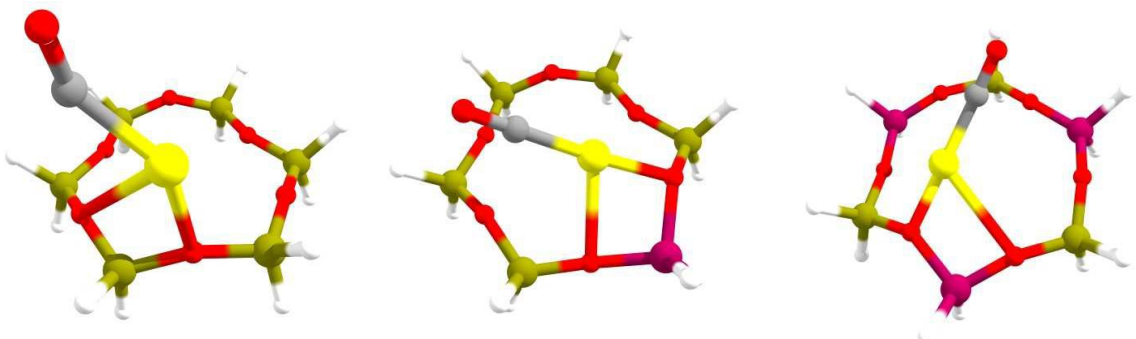

(a) Au^0-CO/FAU (b) Au^+-CO/FAU (c) Au^{3+}-CO/FAU

Figure 3: Optimized structures of CO adsorbed on Au^n/FAU (n=0, +1 and +3).

The optimized structures of H_2O adsorbed on faujasite supported Au monomer, Au^n/FAU (n=0, +1 and +3) via the oxygen atom are shown in Figure 4 and the various structural parameters and the binding energy of H_2O are listed in Table 3. The binding energy of H_2O increases with Au oxidation state and the highest binding energy is observed in Au^{3+}/FAU. The frontier molecular orbitals (Figure S3) show considerable overlap between the d-orbital of Au and p-orbital centered on O atom of H_2O which accounts for the interaction between Au and H_2O. The activation of H_2O indicated by its elongated O-H bonds can be attributed to the H-bonding interaction between the nearest framework O atoms and the H atoms of H_2O which is persistent in the cationic Au systems (shown as dotted bonds in Figure 4).

Table 2: Computed selected geometrical parameters, binding energies and vibrational frequency of CO adsorbed on Au^n/FAU (n=0, +1 and +3).

	Au^0/FAU	Au^+/FAU	Au^{3+}/FAU
	Bond length (Å)		
Au-C	2.07	1.91	1.92
C-O	1.18	1.16	1.16
Au-Si	3.38	3.30	3.19
Au-Al	-	2.96	3.09
Au-O_z	2.82	2.14	2.04
	Vibrational frequency (cm^{-1})		
ν_{C-O}	1867.22	2086.16	2088.14
	Binding energy (eV)		
B.E	3.28	4.38	4.59
	NBO charges		
q(Au)	0.067	0.521	0.525
q(C)	0.356	0.507	0.506

q(O)	-0.445	-0.377	-0.365
q(Al)	-	1.395	1.478
Δq	0.089	-0.13	-0.141

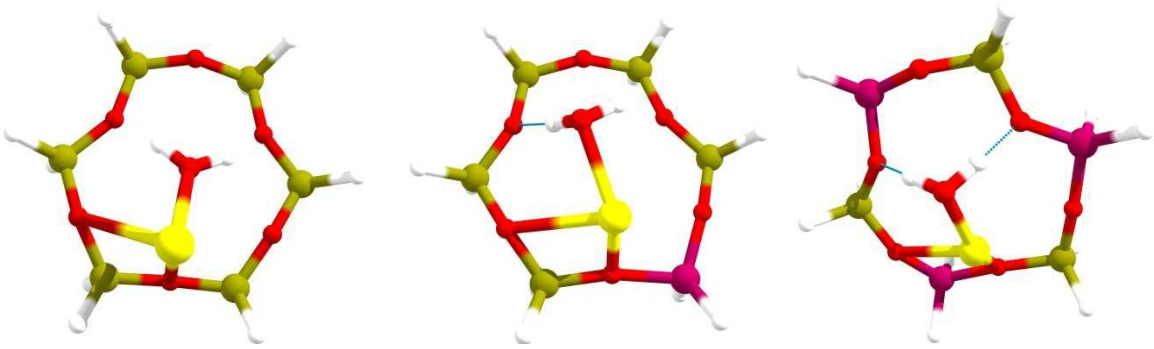

(a) Au^0-H_2O/FAU (b) Au^+-H_2O/FAU (c) Au^{3+}-H_2O/FAU

Figure 4: Optimized structures of H_2O adsorbed on Au^n/FAU (n=0, +1 and +3).

Table 3: Computed bond length (Å) and binding energy (eV) of H_2O adsorbed on Au^n/FAU, n=0, +1 and +3.

	Au^0/FAU	Au^+/FAU	Au^{3+}/FAU
Bond length (Å)			
Au-O	2.26	2.29	2.10
O-H	0.98,0.98	0.98, 1.01	1.00,1.03
$H(H_2O)...O_z$	1.99,2.05	1,68,2.65	1.61,1.86
$Au-O_z$	3.39	2.03	1.98
Binding energy (eV)			
BE	0.51	0.68	0.95
NBO Charges			
q(Au)	-0.070	0.580	0.752
q(O)	-1.000	-0.971	-0.972

q(H)	0.525,0.525	0.526,0.538	0.547,0.549
$q(O_z)$	-1.248	-1.243	-1.222
q(Al)	-	1.409	1.457

3.3. Co-adsorption of CO and H_2O on faujasite supported Au monomer:

The co-adsorption of CO and H_2O on Au^n/FAU (n=0, +1 and +3) can be understood as:

(i) CO adsorbed on H_2O pre-adsorbed Au^n/FAU (n=0, +1 and +3) [$R1^0$, $R1^+$, $R1^{3+}$]

(ii) H_2O adsorbed on CO pre-adsorbed Au^n/FAU (n=0, +1 and +3) [$R1'^0$, $R1'^+$, $R1'^{3+}$].

For optimization of the co-adsorbed configurations, first; optimization of the aggregate with one species adsorbed on the faujasite supported Au monomer was performed which was then followed by optimization of the second species adsorbed on the optimized aggregate. This results in the CO-H_2O co-adsorbed configurations.

In the first case (R1), it has been observed that the adsorption of CO in presence of pre-adsorbed H_2O is favorable in all the oxidation states and the binding energy of CO increases with the Au oxidation state. However, as CO binds with the metal center, it results in the cleavage of the Au-H_2O bond reflected from the elongated Au-O(H_2O) distance in all the oxidation states.

Ito *et al* [59] also indicated that adsorption of CO on Au_2^+ in presence of pre-adsorbed H_2O is assisted by the cleavage of Au-H_2O bond. It is observed that there is apparently no interaction between the CO and H_2O molecules in the three oxidation states. On the other hand, adsorption of H_2O in presence of pre-adsorbed CO is not favorable in Au^0/FAU and Au^{3+}/FAU as reflected from the negative binding energy and also results in the cleavage of Au-CO bond. However, on Au^+/FAU, the adsorption of H_2O is favorable, albeit with low binding energy. Table 4 summarizes the geometrical parameters and the binding energies in the two co-adsorbed

structures. The calculated binding energies indicate that the adsorption of CO on Au^n/FAU (n=0, +1 and +3) in presence of pre-adsorbed H_2O (R1) is preferred over the adsorption of H_2O on CO pre-adsorbed Au^n/FAU (n=0, +1 and +3) (R1′). This can be attributed to the favorable adsorption of CO and much higher binding energies in the former co-adsorbed structure. In the subsequent sections, we discuss the water gas shift reaction on Au^n/FAU (n=0, +1 and +3) starting with these co-adsorbed structures.

Table 4: Computed selected geometrical parameters and the binding energies in the two CO-H_2O co-adsorbed structures, R1 and R1′.

R1				R1′			
	Au^0	Au^+	Au^{3+}		Au^0	Au^+	Au^{3+}
Bond Lengths (Å)				***Bond Lengths (Å)***			
Au-O_z	2.85	2.08	2.02	Au-O_z	2.92	2.01	2.05
C-O	1.17	1.16	1.16	C-O	1.15	1.16	1.15
Au-C(CO)	2.10	1.96	1.91	Au-C(CO)	-	1.91	-
Au-O(H_2O)	3.36	2.69	2.72	Au-O(H_2O)	2.32	2.72	2.65
C(CO)..O(H_2O)	3.81	3.01	2.37	C(CO)..O(H_2O)	3.11	2.40	2.98
H(H_2O)…O_z	1.70	1.82	1.90	H(H_2O)…O_z	2.05	1.94	2.19
O—H	0.98	0.99	0.99	H…OH	0.98	0.97	0.98
Binding energy (eV) of CO				***Binding energy (eV) of H_2O***			
	2.27	3.66	3.84		-0.18	0.29	-1.59

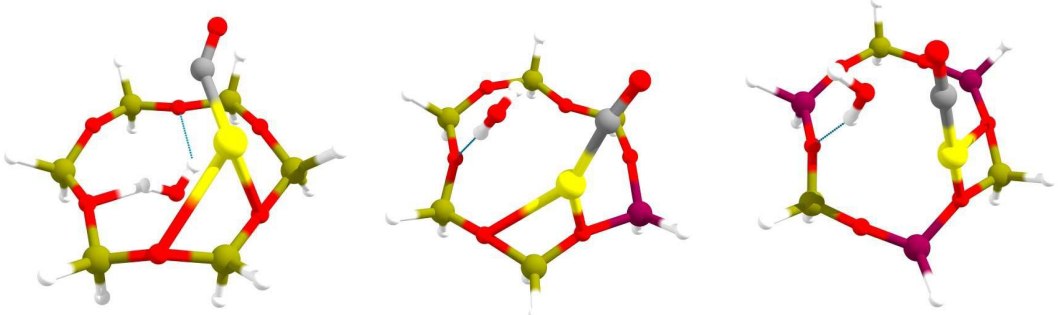

(a) $R1^0$ (b) $R1^+$ (c) $R1^{3+}$

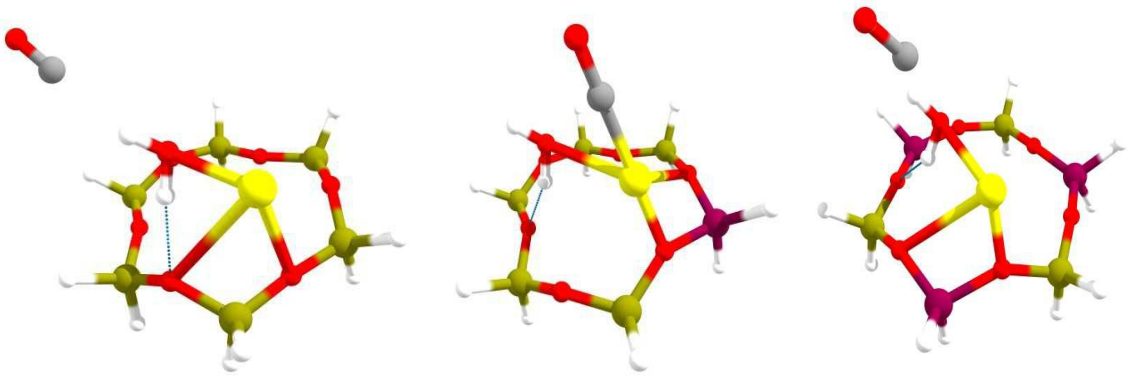

(a) $R1'^{0}$ (b) $R1'^{+}$ (c) $R1'^{3+}$

Figure 5: Optimized structures of CO-H_2O co-adsorbed on Au^n/FAU (n=0, +1 and +3).

3.4. Water gas shift reaction on Au^0/FAU:

We first consider the water gas shift reaction on faujasite supported neutral Au monomer. The energy profile diagram along with the structures of the intermediates and transition states is shown in Figure 6. The geometrical parameters, energy barriers and the single negative vibrational frequency characterizing transition states are summarized in Table 5. The steps involved in the reaction can be outlined as:

$H_2O \longrightarrow H_2O(a)$

$CO \longrightarrow CO(a)$

$H_2O(a) \longrightarrow H(a) + OH(a)$

$CO(a) + OH(a) \longrightarrow COOH(a)$

$COOH(a) \longrightarrow CO_2 + H(a)$

$H(a) + H(a) \longrightarrow H_2$

The reaction commences with the more preferable co-adsorbed structure resulting from CO adsorption on H_2O pre-adsorbed Au^0/FAU ($R1^0$). The next step involves rupture of one O-H bond of H_2O to form an intermediate $I1^0$ such that it contains CO, H and OH. This endothermic step of O-H bond rupture involves a high energy barrier ($TS1^0$) of 2.33 eV and unlike in $R1^0$, the Au-CO bond elongates substantially while two new bonds Au-OH and Au-H emerges in $TS1^0$.

The single negative vibrational frequency of $TS1^0$ appears at -151.46 cm^{-1}. In $I1^0$, formation of Au-OH and Au-H bonds is accompanied by the scission of Au-CO bond. Following this, CO and OH recombine to form a *cis*-COOH intermediate ($I2^0$) via an energy barrier ($TS2^0$) of 0.60 eV. $TS2^0$ is characterized with a single negative vibrational frequency at -530.13 cm^{-1} and involves a moderate interaction between OH and CO as recognized from the decreasing distance to 1.74 Å. The *cis*-COOH intermediate ($I2^0$) is attached to the metal centre via the C atom which is reflected from the substantial overlap of the d-orbital centered on Au and p-orbital of C as illustrated in the frontier molecular orbital (HOMO) shown in Figure 7. The *cis*-COOH intermediate then isomerizes to the more stable *trans*-COOH intermediate ($I3^0$) such that the O-H bond is now directed towards the metal centre and involves a barrier of 0.32 eV ($TS3^0$). Subsequently, the O-H bond elongates to 1.60Å with a concomitant decrease in the OC··OH bond length to 1.29Å in the transition state, $TS4^0$, involved in the formation of CO_2 from the *trans*-COOH intermediate. This barrier is calculated to be 1.78 eV and the single negative vibrational frequency appears at -1042.71 cm^{-1}. The O-H bond subsequently dissociates resulting in the exothermic formation of CO_2 ($I4^0$) and two H atoms attached to the Au metal centre. In the last step, the two H atoms recombine to form H_2 (P^0) and the barrier involved ($TS5^0$) is calculated to be 0.74 eV. $TS5^0$ is characterized by the single negative vibrational frequency that appears at -1285.54 cm^{-1} corresponding to the appearance of a modest interaction between the H atoms. This last reaction step is highly exothermic which implies stable formation of H_2 and thereby regenerating the supported metal atom. It is apparent from the energy profile diagram that the overall reaction is exothermic on Au^0/FAU and the rate limiting step is the dissociation of water which is however, endothermic in nature. Dissociation of water has already been reported as the rate limiting step in the earlier reports and the barrier observed

herein is in fair agreement with that reported previously [60]. The structures of the various intermediates and the transition states involved in the reaction are given in Figure 8.

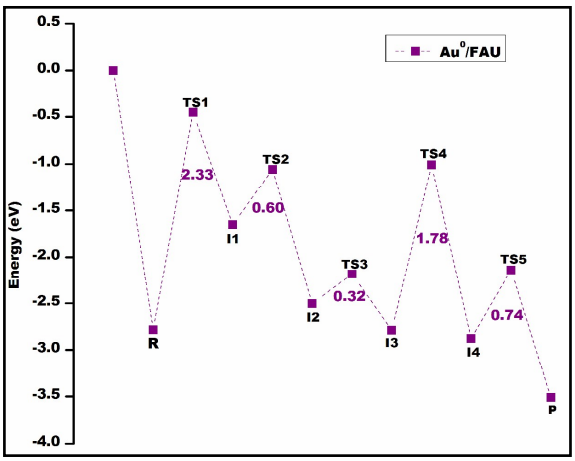

Figure 6: Energy profile diagram for the water gas shift reaction on faujasite supported neutral Au monomer. The energies plotted here refer to the electronic energy without ZPE (Zero Point Energy) corrections.

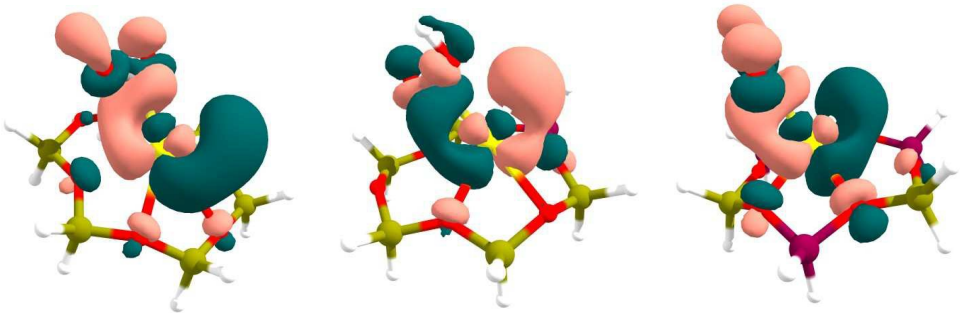

(a) $I2^0$ (HOMO) (b) $I2^+$ (LUMO) (c) $I2^{3+}$ (LUMO+1)

Figure 7: Frontier molecular orbitals illustrating interaction between the Au center and C atom in the *cis*-COOH intermediate ($I2^{0,+,3+}$).

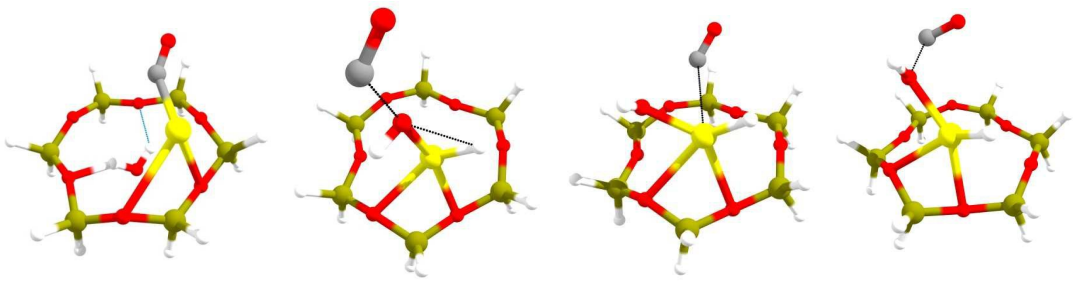

$R1^0$ $TS1^0$ $I1^0$ $TS2^0$

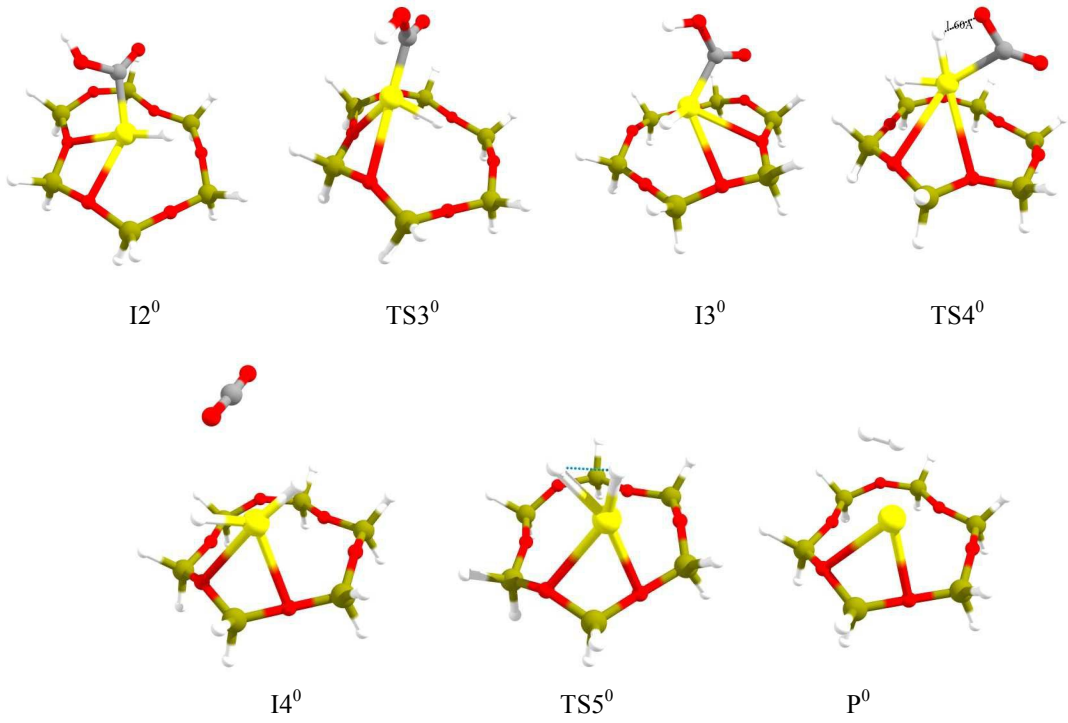

Figure 8: Optimized structures of various intermediates and transition states observed during the reaction on Au^0/FAU.

Table 5: Computed selected geometrical parameters (Å), energy barriers (eV) and single negative vibrational frequencies (cm^{-1}) associated with the transition states in the various steps of the water gas shift reaction on Au^0/FAU.

	Au-O_z	Au-C	Au-OH	Au-H	C-O	OC··OH	H···OH	H-H	ΔE	-ve freq
$R1^0$	2.85	2.10	3.36	-	1.17	-	0.98	-		
$TS1^0$	2.43	4.43	2.27	1.61	1.16	-	2.50	-	2.33	-151.46
$I1^0$	2.87	3.24	2.03	1.60	1.16	-	-	-		
$TS2^0$	2.69	-	2.28	1.58	1.18	1.74	-	-	0.60	-530.13
$I2^0$	2.62	2.14	-	1.64	1.22	1.40	-	-		
$TS3^0$	2.78	1.99	-	1.69	1.21	1.37	-	-	0.32	-116.75
$I3^0$	2.88	2.08	-	1.64	1.22	1.38	-	-		
$TS4^0$	3.24	2.18	-	1.62	1.22	1.29	-	-	1.78	-1042.71
$I4^0$	2.96	-	-	1.63,1.64	1.19	-	-	2.81		
$TS5^0$	2.94	-	-	1.57,2.03	-	-	-	1.45	0.74	-1285.54
P^0	2.90	-	-	-	-	-	-	0.74		

3.5. Water gas shift reaction on Au^{+}/FAU and Au^{3+}/FAU:

We first present the results for the reactivity of Au^{+}/FAU towards water gas shift reaction. As suggested above, the more favorable H_2O-CO co-adsorbed structure ($R1^{+}$) has been considered for studying the water gas shift reaction. Our calculations indicate the presence of a barrier ($TS1^{+}$) as high as 3.71 eV involved in the dissociation of H_2O into H and OH. The H-OH bond of H_2O elongates to 1.79Å in $TS1^{+}$ and the single negative vibrational frequency appears at -863.95 cm^{-1}. The intermediate $I1^{+}$ containing CO, OH and H species is much less stable than $R1^{+}$ which accounts for the observed endothermicity associated with its formation. Further, a weak interaction develops between OH and CO as reflected from the decreasing distance to 1.77Å in $TS2^{+}$ and further to 1.39Å in $I2^{+}$ which results in the recombination of CO and OH to form a *cis*-COOH intermediate. Formation of $I2^{+}$ involves a barrier of 1.94 eV ($TS2^{+}$), is the only step with energy above the entrance channel and thus, is the rate limiting step. Interaction of Au with the C atom in the *cis*-COOH intermediate is depicted by the overlap of d-orbital centered on Au and p-orbital of C as shown in Figure 7. In the subsequent steps, *cis*-COOH isomerizes to the *trans*-COOH ($I3^{+}$) via an energy barrier of 1.40 eV ($TS3^{+}$). The transition state, $TS4^{+}$ involved in the formation of CO2 ($I4^{+}$) from $I3^{+}$ is associated with structural modifications such that the OC····OH bond length reduces with a concomitant elongation of the O-H bond to 1.31Å. As a consequence of this O-H bond elongation, the H atom is now simultaneously bonded to the O atom and the Au centre also reflected from the decreasing Au··H distance to 1.71Å. It can be thus said that, $TS4^{+}$ involves a partially formed CO_2 and the single negative vibrational frequency appears at -1668.03 cm^{-1}. This barrier associated with the formation of CO_2 is calculated to be 1.57 eV. In the next step, the distance between the H atoms reduces to 1.20Å in $TS5^{+}$ which indicates that a moderate interaction develops between them and the barrier involved in the formation

of H_2 is calculated to 0.33 eV. The overall reaction on Au^+/FAU is endothermic as apparent from the energy profile diagram depicted in Figure 9. The geometrical parameters, energy barriers involved in the different steps and the negative vibrational frequencies associated with the transition states are summarized in Table 6.

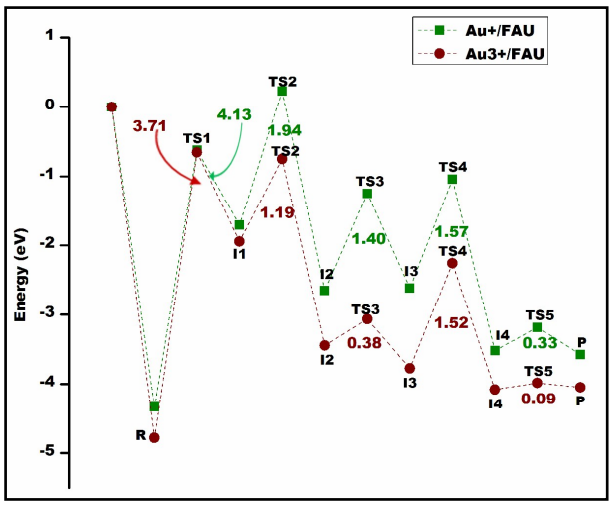

Figure 9: Energy profile diagram for the water gas shift reaction on faujasite supported cationic Au monomer (Au^+ and Au^{3+}). The energies plotted here refer to the electronic energy without ZPE (Zero Point Energy) corrections.

On Au^{3+}/FAU, the first step i.e the dissociation of H_2O into OH and H ($I1^{3+}$) from the H_2O-CO co-adsorbed structure ($R1^{3+}$) involves still higher barrier (4.13 eV) and is endothermic. This barrier involved in water dissociation in the cationic systems is comparatively much higher as compared to that observed for the neutral monomer. In the transition state, $TS1^{3+}$, the Au-CO bond ruptures while Au-OH and Au-H appears and the single negative vibrational frequency appears at -123.33 cm^{-1}. Further, the distance between OH and CO decreases to 1.56Å which implies that a modest interaction develops in $TS2^{3+}$. This barrier involved in the formation of *cis*-COOH intermediate ($I2^{3+}$) is calculated to be 1.19 eV and the single negative vibrational frequency appears at -500.27 cm^{-1}. The CO···OH distance decreases further to 1.36Å such that CO and OH recombine to form a *cis*-COOH intermediate. However, unlike in Au^+/FAU, this step of COOH formation from $I1^{3+}$ is below

the entrance channel and is exothermic which indicates that the *cis*-COOH intermediate is more stable than the intermediate $I1^{3+}$. The interaction of Au with the C atom of COOH intermediate is depicted by the overlap of the Au-d-orbital and C-p-orbital as illustrated in Figure 7. Isomerisation of $I2^{3+}$ to *trans*-COOH ($I3^{3+}$) intermediate entails a barrier of 0.38 eV ($TS3^{3+}$) and the negative frequency appears at -216.80 cm^{-1}. The O-H bond elongates to 1.21Å while the Au-H distance decreases to 1.89Å in the transition state, $TS4^{3+}$ observed in the formation of CO_2 ($I4^{3+}$) from $I3^{3+}$. The CO···OH distance decreases to 1.27Å and the O-C-O angle is observed to 156.81° which represents a partially formed CO_2. The single negative frequency appears at -1627.16 cm^{-1}. With the formation of CO_2 ($I4^{3+}$), two H atoms are now attached to the Au centre and the distance between them is 1.93Å which indicates lack of any interaction between them. The distance however, reduces to 1.12Å implying appearance of interaction between the H atoms in $TS5^{3+}$ and the single negative vibrational frequency appears at -861.79 cm^{-1}. This barrier involved in the formation of H_2 is calculated to be 0.09 eV. The overall reaction is endothermic as reflected from the energy profile diagram shown in Figure 8. Table 7 summarizes the geometrical parameters, energy barriers involved in the different steps and the negative vibrational frequencies associated with the transition states.

4. Conclusion

Hybrid quantum mechanics/molecular mechanics calculations have carried out to investigate the activity of faujasite supported neutral and cationic Au monomer towards water-gas shift reaction. It has been observed that CO adsorption on Au^n/FAU (n=0, +1 and +3) in presence of pre-adsorbed H_2O is more favorable than the adsorption of H_2O on Au^n/FAU (n=0, +1 and +3) in presence of pre-adsorbed CO and thus, has been appraised as the starting configuration for investigating the reaction mechanism. The reaction mechanism

involves the formation of a carboxyl intermediate in all the oxidation states from the recombination of CO and OH. However, carboxyl formation step is above the entrance channel in Au^{+}/FAU and is thus, the rate limiting step. The overall reaction is found to be endothermic in both the cationic systems while is exothermic in Au^{0}/FAU. Comparing the activity of the three Au monomer species, it is observed that neutral Au exhibits better catalytic activity towards water-gas shift reaction. The dissociation of H_2O into OH and H is the rate limiting step in Au^{0}/FAU. Substantially high barriers associated with the cationic systems and endothermicity of the reaction will limit their catalytic activity. However, reducing the water dissociation barrier observed in the neutral monomer will improve the catalytic activity further.

Table 5: Computed selected geometrical parameters (Å), energy barriers (eV) and the single negative vibrational frequencies (cm^{-1}) associated with the transition states in the various steps of the water gas shift reaction on Au^{+}/FAU.

	Au-O_z	Au-C	Au-OH	Au-H	C-O	OC··OH	H···OH	H-H	ΔE	-ve freq
$R1^{+}$										
$TS1^{+}$	2.35	3.04	2.10	1.54	1.16	-	1.79	-	3.71	-863.95
$I1^{+}$	2.07	3.56	2.03	1.53	1.16	-	-	-		
$TS2^{+}$	2.57	2.50	2.25	1.52	1.18	1.77	-		1.94	-529.55
$I2^{+}$	2.51	2.04	-	1.56	1.21	1.39	-	-		
$TS3^{+}$	2.43	2.05	-	1.55	1.21	1.34	-	-	1.40	-1196.30
$I3^{+}$	2.54	2.06	-	1.57	1.21	1.36	-	-		
$TS4^{+}$	2.46	2.46	-	1.61	1.18	1.28	-	-	1.57	-1668.03
$I4^{+}$	2.23	-	-	1.55,156	1.19	-	-	2.41		
$TS5^{+}$	2.28	-	-	1.62	-	-	-	1.20	0.33	-965.11
P^{+}	2.28	-	-	1.80	-	-	-	0.85		

Table 6: Computed selected geometrical parameters (Å), energy barriers (eV) and the single negative vibrational frequencies (cm^{-1}) associated with the transition states in the various steps of the water gas shift reaction on Au^{3+}/FAU.

	Au-O_z	Au-C	Au-OH	Au-H	C-O	OC··OH	H···OH	H-H	ΔE	-ve freq
$R1^{3+}$										
$TS1^{3+}$	2.33	3.46	1.99	1.55	1.15	-	2.29	-	4.13	-123.33
$I1^{3+}$	1.22	3.37	1.94	1.53	1.15	-	-	-		
$TS2^{3+}$	2.13	2.65	2.20	1.54	1.19	1.56	-	-	1.19	-500.27
$I2^{3+}$	2.31	2.02	-	1.56	1.23	1.36	-	-		
$TS3^{3+}$	2.33	2.04	-	1.57	1.22	1.36	-	-	0.38	-216.80
$I3^{3+}$	2.32	2.05	-	1.58	1.21	1.34	-	-		
$TS4^{3+}$	2.33	2.53	-	1.57	1.18	1.27	1.21	-	1.52	-1627.16
$I4^{3+}$	2.25	-	-	1.55,1.56	1.19	--	-	1.93		
$TS5^{3+}$	2.28	-	-	1.65,1.63	-	-	-	1.12	0.09	-861.79
P^{3+}	2.34			1.76,1.78	-	-	-	0.84		

The conclusions drawn from this study with a simple model of zeolite supported Au catalyst may be inherent for understanding the catalytic activity of larger realistic catalytic system so as to apprehend the mechanism involved. Further, designing improved catalysts with enhanced potential for water gas shift reaction will open up a new dimension for water gas shift reaction catalysts.

References

[1] T. R. Reina, W. Xu, S. Ivanova, M. Á. Centeno, J. Hansonb, J. A. Rodriguez, J. A. Odriozola, *Catalysis Today*, 2013, **205**, 41.

[2] S. Colussi, L. Katta, F. Amoroso, R. J. Farrauto, A. Trovarelli, *Catal. Commun.*, 2014, **47**, 63.

[3] W. Denga, C. Carpenter, N. Yi, M. Flytzani-Stephanopoulos, *Topics in Catalysis*, 2007, **44**, 199.

[4] C. M. Kalamaras, D. D. Dionysiou, A. M. Efstathiou, *ACS Catal.*, 2012, **2**, 2729.

[5] C. Wen, Y. Zhu,Y. Ye,S. Zhang, F. Cheng, Y. Liu, P.Wang, F. (F.) Tao, *ACS Nano*, 2012, **6**, 9305.

[6] Y. Wang, Y. Zhai, D. Pierre, M. Flytzani-Stephanopoulos, *Appl. Catal. B: Environ.*, 2012, **127**, 342.

[7] R. Sia, J. Raitanob, N. Yia, L. Zhang, Siu-W. Chanb, M. Flytzani-Stephanopoulos, *Catal. Today*, 2012, **180**, 68.

[8] A. B. Vidal, P. Liu, *Phys. Chem. Chem. Phys.*, 2012, **14**, 16626.

[9] H. Wei, C. Gomez, R. J. Meyer, *Top. Catal.*, 2012, **55**, 313.

[10] Y. Chen, H. Wang, R. Burch, C. Hardacre, P. Hu, *Faraday Discuss.*, 2011, **152**, 121.

[11] P. Liu, *J. Chem. Phys.*, 2010, **133**, 204705/1.

[12] P. Liu, J. A. Rodriguez, *J. Chem. Phys,*. 2007, **126**, 164705/1.

[13] B. K. Min, C. M. Friend, *Chem. Rev.*, 2007, **107**, 2709.

[14] B. Jørgensen, S. E. Christiansen, M. L. D. Thomsen, C. H. Christensen, *J. Catal*., 2007, **251**, 332.

[15] G.Vilé,J.Pérez-Ramírez, *Nanoscale*, 2014, **6**, 13476.

[16] D. Andreeva, V. Idakiev, T. Tabakova, A. Andreev, *J. Catal.*, 1996, **158**, 354.

[17] D. Andreeva, V. Idakiev, T. Tabakova, A. Andreev, R. Giovanoli, *Appl.Catal. A: General*, 1996, **134**, 275.

[18] L. F. Allard, A. Borisovich, W. Deng, R. Si, M. Flytzani-Stephanopoulos, S. H. Overbury, *J. Electron Microsc.*, 2009, **58**, 199.

[19] L. F. Allard, M. Flytzani-Stephanopoulos, S. H. Overbury, *Microsc. Microanal.*, 2010, **16**, 375.

[20] Q. Fu, A. Weber, M. Flytzani-Stephanopoulos, *Catal. Lett.*, 2001, **77**, 87.

[21] Q. Fu, S. Kudriavtseva, H. Saltsburg, M. Flytzani-Stephanopoulos, *Chem. Eng. J.*, 2003, **93**, 41.

[22] Q. Fu, W. Deng, H. Saltsburg, M. Flytzani-Stephanopoulos, *Appl. Catal. B: Environmental*, 2005, **56**, 57.

[23] W. Deng, A. I. Frenkel, R. Si, M. Flytzani-Stephanopoulos, *J. Phys. Chem. C*, 2008, **112**, 12834.

[24] C. Wen, Y. Zhu, Y. Ye, S. Zhang, F. Cheng, Y. Liu, P. Wang, F.(Feng) Tao, *ACS Nano*, 2012, **6**, 9305.

[25] R. Si, J. Tao, J. Evans, J. B. Park, L. Barrio, J. C. Hanson, Y. Zhu, J. Hrbek, J. A. Rodriguez, *J. Phys. Chem. C*, 2012, **116**, 23547.

[26] J. A. Rodriguez, S. D. Senanayake, D. Stacchiola, P. Liu, J. Hrbek, *Acc. Chem. Res.*, 2014, **47**, 773.

[27] D. C. Grinter, C. Muryn, B. Santos, B.-J. Shaw, T. O. Menteş, A. Locatelli, G. Thornton, *J. Phys. Chem. C*, 2014, **118**, 19194.

[28] D. Tibiletti, A. Amieiro-Fonseca, R. Burch, Y. Chen, J. M. Fisher, A. Goguet, C. Hardacre, P. Hu, D. Thompsett, *J. Phys. Chem. B*, 2005, **109**, 22553.

[29] Y. Chen, H. Wang, R. Burch, C. Hardacre, P. Hu, *Faraday Discuss.*, 2011, **152**, 121.

[30] H. Sakurai, A. Ueda, T. Kobayashi, M. Haruta, *Chem. Commun.*, 1997, 271.

[31] J. A. Rodríguez, J. Evans, J. Graciani, J.-B. Park, P. Liu, J. Hrbek, J. Fdez. Sanz, *J. Phys. Chem. C*, 2009, **113**, 7364.

[32] W. D. Williams, M. Shekhar,W.-S. Lee, V. Kispersky, W. N. Delgass, F. H. Ribeiro, S. M. Kim, E. A. Stach, J. T. Miller, L. F. Allard, *J. Am. Chem. Soc.*, 2010, **132**, 14018.

[33] M. Shekhar, J. Wang, W.-S. Lee, W. D. Williams, S. M. Kim, E. A. Stach, J. T. Miller, W. N. Delgass, F. H. Ribeiro, *J. Am. Chem. Soc.*, 2012, **134**, 4700.

[34] J. Wang, V. F. Kispersky, W. N. Delgass, F. H. Ribeiro, *J. Catal.*, 2012, **289**, 171.

[35] M. Yang, L. F. Allard, M. Flytzani-Stephanopoulos, *J. Am. Chem. Soc.*, 2013, **135**, 3768.

[36] J. A. Rodriguez, P. Liu, J. Hrbek, J. Evans, M. Pérez, *Angew. Chem. Int. Ed.*, 2007, **46**, 1329.

[37] A. Goguet, R. Burch,Y. Chen, C. Hardacre, P. Hu, R. W. Joyner, F. C. Meunier, B. S. Mun, D. Thompsett, D. Tibiletti, *J. Phys. Chem. C*, 2007, **111**, 16927.

[38] J. Li, N. Ta, W. Song, E. Zhan, W. Shen, *Gold Bull.*, 2009, **42**, 48.

[39] B. A. Lenite, C. Galletti, S. Specchia, *Int. J. Hydrogen Energy*, 2011, **36**, 7750.

[40] J. D. Lessard, I. Valsamakis, M. Flytzani-Stephanopoulos, *Chem. Commun.,* 2012, **48**, 4857.

[41] F. Menegazzo, F. Pinna, M. Signoretto, V. Trevisan, F. Boccuzzi, A. Chiorino, M. Manzol, *Chem. Sus. Chem.*, 2008, **1**, 320.

[42] M. M. Mohamed and M. Ichikawa, *J. Colloid Interface Sci.*, 2000, **232**, 381.

[43] M. M. Mohamed, T. M. Salama, M. Ichikawa, *J. Colloid Interface Sci.*, 2000, **224**, 366.

[44] Q. Fu, H. Saltsburg, M. Flytzani-Stephanopoulos, *Science*, 2003, **301**, 935.

[45] D. Tibiletti, A. Amieiro-Fonseca, R. Burch, Y. Chen, J. M. Fisher, A. Goguet, C. Hardacre, P. Hu, D. Thompsett, *J. Phys. Chem. B*, 2005, **109**, 22553.

[46] W. Deng, J. De Jesus, H. Saltsburg, M. Flytzani-Stephanopoulos, *Appl. Catal. A: General*, 2005, **291**, 126.

[47] Z.-P. Liu, S. J. Jenkins, D. A. King, *Phys. Rev. Lett.*, 2005, **94**, 196102/1.

[48] Xiao-F. Yang, A. Wang, B. Qiao, J. Li, J. Liu, T. Zhang, Acc. Chem. Res., 2013, **46**, 1740.

[49] J. Lin, A. Wang, B. Qiao, X. Liu, X. Yang, X. Wang, J. Liang, J. Li, J. Liu, T. Zhang, *J. Am. Chem. Soc.* 2013, **135**, 15314.

[50] J. R. Shoemaker, L. W. Burggraf, M. S. Gordon, *J. Phys. Chem. A,* 1999, **103**, 3245.

[51] M. W. Schmidt, K. K. Baldridge, J. A. Boatz, S. T. Elbert, M. S. Gordon, J. H. Jensen, S. Koseki, N. Matsunga, K. A. Nguyen, S. J. Su, T. L. Windus, M. Dupuis, J. A. Montgomery, *J. Comput. Chem.*, 1993, **14**, 1347.

[52]. P. Culot, G. Dive, V. H. Nguyen, J. M. Ghuysen, *Theor. Chim. Acta*, 1992, **82**, 189.

[53] A. D. Becke, *J. Chem. Phys.,* 1993, **98**, 5648.

[54] C. Lee, W. Yang, R. G. Parr, *Phys. Rev. B*, 1988, **37**, 785.

[55] M. J. Frisch, J. A. Pople, J. S. Binkley, *J. Chem. Phys*., 1984, **80**, 3265.

[56] P. J. Hay, W. R. Wadt, *J. Chem. Phys.*, 1985, **82**, 270.

[57] N. L. Allinger, Y. H. Yuh, J. H. Lii, *J. Am. Chem. Soc.*, 1989, **111**, 8551.

[58] J. C. Fierro-Gonzalez, and B. C. Gates, *J. Phys. Chem. B*, 2004, **108**, 16999.

[59] T. Ito, G. N. Patwari, M. Arakawa, A. Terasaki, *J. Phys. Chem. A*, 2014, **118**, 8293.

[60] Y. Wang, D. Zhang, R. Zhu, C. Zhang, C. Liu, *J. Phys. Chem. C*, 2009, **113**, 6215.